Real-Time Propagation of the Reduced One-Electron Density Matrix in Atom-Centered Orbitals: Application to Electron Injection Dynamics in Dye-Sensitized TiO_2 Clusters

Zhenyu Guo and WanZhen Liang*

Hefei National Laboratory for Physical Science at Microscale, and Department of Chemical Physics, University of Science and Technology of China, Hefei 230026, People's Republic of China

Yi Zhao*

State Key Laboratory of Physical Chemistry of Solid Surfaces, and Department of Chemistry, Xiamen University, Xiamen, 361005, People's Republic of China

GuanHua Chen

Department of Chemistry, The University of Hong Kong, Pokfulam Road, Hong Kong, People's Republic of China

Received: March 7, 2008; Revised Manuscript Received: July 23, 2008

The ultrafast electron-transfer (ET) processes in three dye-sensitized TiO_2 systems (pycooh−, catechol−, and alizarin−) are studied by using the real-time time-dependent density functional theory (RT-TDDFT). TiO_2 cluster models are used to substitute TiO_2 nanocrystals in order to check the quantum size effect on ET. The initial-state geometrical optimization for the individual constituents and coupled systems and the subsequent calculations for IR spectra and the density of states (DOS) are performed at the B3LYP/Lanl2dz theory level. The calculated IR spectra, the DOS, and the low-lying excited states reveal that the couplings between three dyes and TiO_2 clusters are very strong so that an ultrafast electron injection from the excited dyes to TiO_2 clusters is favored. By following the electronic motion of coupled systems after the photoexcitation of adsorbates in real time without allowing the nuclei to move, we predict an electronic injection time of a few femtoseconds for the present finite systems, which is slightly longer than the experimental measurements and other theoretical predications for the ET time on the same dye-sensitized bulk TiO_2 systems due to the small clusters used in our simulation. We find that the ET time is appreciably dependent on the cluster size when the cluster is quite small. However, the size effects on ET time reduce dramatically as the cluster size reaches to a moderate middle size, for example, $(TiO_2)_{14}$. The electron−nuclear coupled movement does not play a significant role in the initial ET process in these three systems. The effects of different initial excited states on electronic dynamics are also discussed.

1. Introduction

Light-driven heterogeneous electron transfer (ET) is a fundamental process that plays an important role in interfacial photoprocesses, particularly in photoelectrochemistry,[1−6] photocatalysis,[7−9] and molecular electronics for dye-sensitized solar cells (DSSCs).[10,11] DSSC assembles organic dyes with inorganic semiconductor nanocrystals such as TiO_2 and realizes the optical absorption and charge-separation processes. For the dye-sensitized systems, one can simplistically think of the photoinduced ET as an electron being transferred from the excited states of chromophores to the conductive bands of nanocrystals. Visible light excites the dye-sensitizer molecules from the ground state to an excited-state which is resonant with the TiO_2 conduction band. The excited electrons are then transferred to the semiconductor on an ultrafast time scale. A series of experimental studies has given evidence that the time of the electron injection from chromophore to nanocrystal in some sensitized systems can be as short as a few femtoseconds.[12−16] This ultrafast ET dynamics cannot be well explained by the traditional ET rate theory and requires a time-resolved femtosecond or subfemtosecond laser technique or real-time theoretical study.

Extensive theoretical studies on such ultrafast dynamics in real time have been performed (see, e.g., refs 17−21). An excellent review about these works has been given by Duncan and Prezhdo in ref 22 recently. With different approximated strategies, the current theoretical approaches are classified into two categories. One is a fully quantum mechanical description for electron and nuclear movement with simple interfacial models.[17−19] In such an approach, the electronic Hamiltonian is commonly taken as the Newns−Anderson model, and the nuclear is considered as a collection of harmonic oscillators. The other strategy implements electron movement quantum mechanically but nuclear movement classically, the so-called quantum−classical approach.[20,21]

In previous theoretical studies, TiO_2 is usually assumed as an extending bulk system so that the periodic boundary condition is used. The rates and yields of ET reactions are determined by the energies of chromophores and semiconductor donor−acceptor states and by the couplings between these states.[23] These two quantities are closely related to the nanocrystal sizes. Normally, rutile, anatase, and brookite crystals are the main forms of TiO_2 in nature.[24] The anatase phase becomes more stable than the

* To whom correspondence should be addressed. E-mail: liangwz@ustc.edu.cn (W.L.); yizhao@xmu.edu.cn.

10.1021/jp802007h CCC: $40.75
Published on Web 09/30/2008

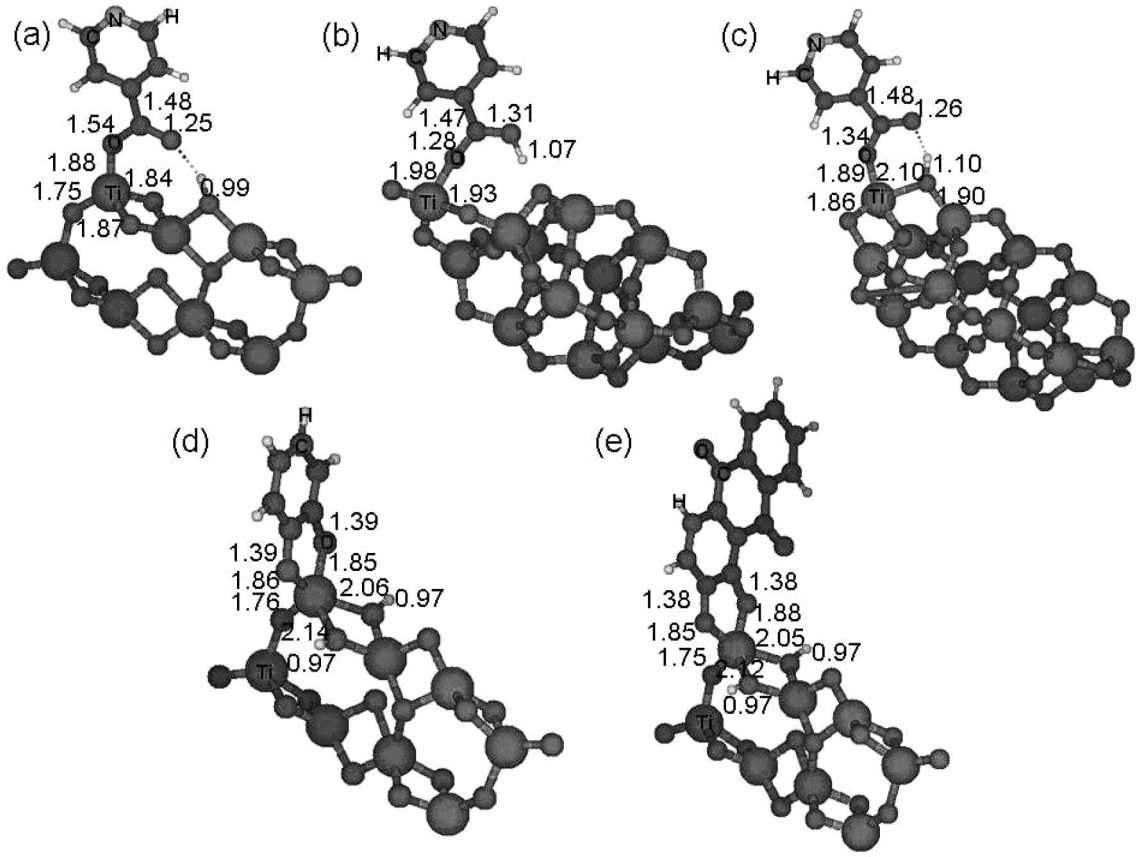

Figure 1. Geometry of five dye−(TiO_2)(cluster) complexes. Atoms H, C, O, N, and Ti are marked on the corresponding spheres. All of the bond lengths are in angstroms; (a) pycooh−$(TiO_2)_8$, (b) pycooh−$(TiO_2)_{14}$, (c) pycooh−$(TiO_2)_{16}$, (d) catechol−$(TiO_2)_8$, (e) alizarin−$(TiO_2)_8$.

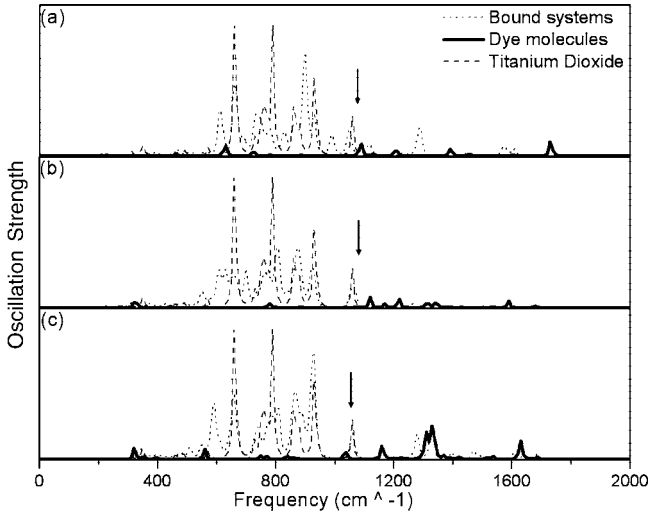

Figure 2. Infrared spectra of (a) pycooh−$(TiO_2)_8$, (b) catechol−$(TiO_2)_8$, and (c) alizarin−$(TiO_2)_8$. The dashed, solid, and dotted lines represent $(TiO_2)_8$, the free dye molecule, and the dye−$(TiO_2)_8$ complex, respectively. The arrows indicate the collective vibrations of the dye molecule and TiO_2 that correspond to the ET.

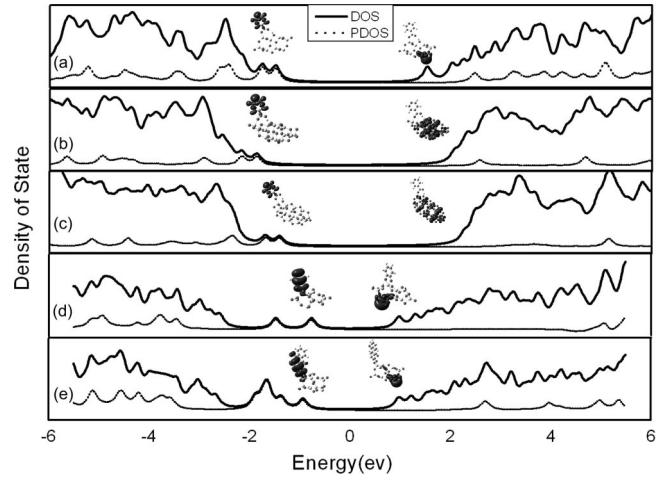

Figure 3. DOS of (a) pycooh−$(TiO_2)_8$, (b) pycooh−$(TiO_2)_{14}$, (c) pycooh−$(TiO_2)_{16}$, (d) catechol−$(TiO_2)_8$, and (e) alizarin−$(TiO_2)_8$. The solid and dashed lines represent DOS and PDOS(dye fragments), respectively.

rutile phase when the sizes of TiO_2 are smaller than about 14 nm.[25] With small enough crystals, the quantum size effect is obvious, in contrast to the bulk. It will be interesting to see how the quantum size effect of the small crystals affects the ET process. In the present work, we therefore use cluster models to substitute TiO_2 nanocrystals in order to check this quantum size effect and get the balance between computational costs and reliability as well.

We choose three dye-sensitized systems, isonicotinic acid (pycooh), catechol, and alizarin to bind up with TiO_2 clusters. Then, the electronic structures and electron dynamics of three coupled systems are studied by the first-principles density functional theory. To check the coupling strength between the dyes and TiO_2 cluster, we calculate the IR spectra, density of states (DOS), and the low-lying excited states of both coupled systems and sole TiO_2 clusters. The calculated results reveal that the dyes couple strongly with TiO_2 clusters, which makes it questionable to explicitly split the adsorbate and TiO_2 cluster as a donor and an acceptor. In the present work, we consider

TABLE 1: The Calculated Low-Lying Excited States of $(TiO_2)_{8/14/16}$ Clusters[a]

state	excited energy	orbitals contributing to excitation
	$(TiO_2)_8$	
1	3.1620(0.0001)	$0.9874\|H \rightarrow L\rangle$
2	3.1647(0.0001)	$0.9884\|H - 1 \rightarrow L\rangle$
3	3.1846(0.0001)	$0.2284\|H - 4 \rightarrow L\rangle + 0.2388\|H - 1 \rightarrow L + 2\rangle$ $+0.8737\|H \rightarrow L + 1\rangle + 0.2773\|H \rightarrow L + 2\rangle$
4	3.1880(0.0014)	$-0.2588\|H \rightarrow L + 1\rangle + 0.9216\|H \rightarrow L + 2\rangle$
5	3.1909(0.0006)	$-0.5622\|H - 1 \rightarrow L + 1\rangle - 0.7264\|H - 1 \rightarrow L + 2\rangle$ $-0.2822\|H \rightarrow L + 1\rangle$
	$(TiO_2)_{14}$	
1	3.9286(0.0125)	$0.2771\|H - 5 \rightarrow L\rangle + 0.4027\|H - 1 \rightarrow L + 1\rangle$ $-0.2261\|H - 1 \rightarrow L + 8\rangle + 0.6756\|H \rightarrow L\rangle$ $+0.2804\|H \rightarrow L + 5\rangle$
2	3.9436(0.0000)	$0.5863\|H - 1 \rightarrow L\rangle + 0.3292\|H - 1 \rightarrow L + 5\rangle$ $+0.4858\|H \rightarrow L + 1\rangle - 0.2618\|H \rightarrow L + 8\rangle$
3	3.9954(0.0000)	$+0.5463\|H - 4 \rightarrow L\rangle + 0.3390\|H - 3 \rightarrow L + 1\rangle$ $+0.6224\|H - 2 \rightarrow L\rangle$
4	4.0209(0.0003)	$0.2711\|H - 9 \rightarrow L\rangle + 0.2166\|H - 6 \rightarrow L\rangle$ $+0.3308\|H - 4 \rightarrow L + 1\rangle + 0.6395\|H - 3 \rightarrow L\rangle$ $+0.4418\|H - 2 \rightarrow L + 1\rangle$
5	4.0367(0.0028)	$-0.2586\|H - 7 \rightarrow L + 1\rangle + 0.6400\|H - 5 \rightarrow L\rangle$ $-0.2738\|H - 1 \rightarrow L + 8\rangle - 0.3685\|H \rightarrow L + 5\rangle$
	$(TiO_2)_{16}$	
1	3.7733(0.0041)	$0.5859\|H - 2 \rightarrow L\rangle - 0.3615\|H - 2 \rightarrow L + 1\rangle$ $+0.2678\|H - 2 \rightarrow L + 2\rangle - 0.4884\|H - 1 \rightarrow L\rangle$ $-0.3012\|H - 1 \rightarrow L + 1\rangle + 0.2232\|H - 1 \rightarrow L + 1\rangle$
2	3.7733(0.0041)	$0.4884\|H - 2 \rightarrow L\rangle - 0.3012\|H - 2 \rightarrow L + 1\rangle$ $+0.2232\|H - 2 \rightarrow L + 2\rangle + 0.5859\|H - 1 \rightarrow L\rangle$ $+0.3615\|H - 1 \rightarrow L + 1\rangle - 0.2678\|H - 1 \rightarrow L + 1\rangle$
3	3.7914(0.0000)	$-0.8926\|H \rightarrow L\rangle$
4	3.8839(0.0000)	$-0.2248\|H - 4 \rightarrow L + 1\rangle + 0.6189\|H - 3 \rightarrow L\rangle$ $+0.3004\|H \rightarrow L + 1\rangle - 0.5334\|H \rightarrow L + 2\rangle$
5	3.9459(0.0000)	$-0.9157\|H \rightarrow L + 3\rangle$

[a] The orbital contributions for each state are given. The values in parentheses denote the oscillator strengths.

TABLE 2: The calculated low-lying excited states of free and bound pycooh.

state	excited energy (eV)	orbitals contributing to excitation
	pycooh	
1	4.0339(0.0022)	$-0.9921\|H \rightarrow L\rangle$
2	4.4449(0.0000)	$-0.9818\|H - 2 \rightarrow L\rangle$
3	4.8217(0.0405)	$0.3196\|H - 3 \rightarrow L + 1\rangle + 0.9457\|H - 1 \rightarrow L\rangle$
4	5.1671(0.0000)	$-0.9973\|H \rightarrow L + 1\rangle$
5	5.7766(0.1757)	$0.9372\|H - 3 \rightarrow L\rangle - 0.3224\|H - 1 \rightarrow L + 1\rangle$
	pycooh$-(TiO_2)_8$	
1	2.7989(0.0000)	$0.9997\|H \rightarrow L\rangle$
2	3.0633(0.0000)	$0.9996\|H - 1 \rightarrow L\rangle$
3	3.2801(0.0000)	$0.9962\|H \rightarrow L + 1\rangle$
4	3.3063(0.0038)	$0.9547\|H - 2 \rightarrow L\rangle$
5	3.3859(0.0057)	$0.8962\|H - 5 \rightarrow L\rangle - 0.2509\|H - 2 \rightarrow L\rangle$
	pycooh$-(TiO_2)_{14}$	
1	3.4692(0.0012)	$-0.8378\|H \rightarrow L + 5\rangle$
2	3.6560(0.0000)	$0.9608\|H \rightarrow L\rangle$
3	3.8091(0.0000)	$0.9398\|H \rightarrow L + 1\rangle + 0.2506\|H \rightarrow L + 2\rangle$
4	3.8850(0.0000)	$-0.2471\|H \rightarrow L + 1\rangle + 0.9580\|H \rightarrow L + 2\rangle$
5	3.9228(0.0003)	$0.9667\|H - 1 \rightarrow L\rangle + 0.2383\|H - 1 \rightarrow L + 1\rangle$
	pycooh$-(TiO_2)_{16}$	
1	3.4259(0.0004)	$0.9282\|H \rightarrow L\rangle + 0.3053\|H \rightarrow L + 2\rangle$
2	3.6247(0.0002)	$-0.3663\|H \rightarrow L\rangle + 0.8264\|H \rightarrow L + 2\rangle$
3	3.6314(0.0001)	$-0.8863\|H \rightarrow L\rangle - 0.2574\|H \rightarrow L + 3\rangle$ $+0.2586\|H \rightarrow L + 6\rangle$
4	3.6736(0.0003)	$-0.9205\|H - 1 \rightarrow L\rangle + 0.3362\|H - 1 \rightarrow L + 2\rangle$
5	3.6789(0.0002)	$0.2183\|H \rightarrow L + 1\rangle - 0.3362\|H \rightarrow L + 2\rangle$ $+0.8709\|H \rightarrow L + 3\rangle$

the adsorbate and TiO_2 cluster as a "supermolecule". Therefore, the electronic dynamics is considered as an intramolecular ET. A RT-TDDFT approach, proposed by us recently,[26,27] is then used to describe electron dynamics. We follow in time the evolution of the atomic electron population until the onset of nuclear-motion-induced relaxation terminates the purely electronic coherent motion. In present RT-TDDFT simulation, the nuclear motion is not incorporated. It is known that the nuclear motion should be incorporated if characteristic times of electronic and nuclear motions are on the same order. For the present systems, however, our vibrational analysis shows that the shortest vibrational period is about 33 fs, which is longer than

TABLE 3: The Calculated Low-Lying Excited States of Free and Bound Catechol

state	excited energy (eV)	orbitals contributing to excitation
	Catechol	
1	5.0914(0.0378)	$0.8713\|H \rightarrow L\rangle + 0.4793\|H - 1 \rightarrow L + 2\rangle$
2	5.8585(0.0414)	$0.8581\|H \rightarrow L + 1\rangle - 0.4954\|H - 1 \rightarrow L\rangle$
3	6.0473(0.0000)	$0.9890\|H \rightarrow L + 2\rangle$
4	6.7677(0.3399)	$0.4703\|H \rightarrow L + 1\rangle + 0.8223\|H - 1 \rightarrow L\rangle$
5	6.9075(0.0000)	$0.9286\|H -1 \rightarrow L + 2\rangle - 0.3224\|H \rightarrow L + 3\rangle$
	Catechol$-(TiO_2)_8$	
1	1.3519(0.0009)	$0.8130\|H \rightarrow L\rangle - 0.5637\|H \rightarrow L + 1\rangle$
2	1.4444(0.0010)	$0.5811\|H \rightarrow L\rangle + 0.7865\|H \rightarrow L + 1\rangle$
3	1.8747(0.0008)	$0.9329\|H \rightarrow L + 2\rangle$
4	1.9403(0.0006)	$0.8722\|H \rightarrow L + 3\rangle + 0.3794\|H \rightarrow L + 4\rangle$ $+0.2178\|H \rightarrow L + 6\rangle$
5	2.0784(0.0001)	$0.9347\|H - 1 \rightarrow L\rangle - 0\ .3341\|H - 1 \rightarrow L + 1\rangle$

TABLE 4: The Calculated Low-Lying Excited States of Free and Bound Alizarin

state	excited energy (eV)	orbitals contributing to excitation
	Alizarin	
1	2.7492(0.0022)	$0.9759\|H - 1 \rightarrow L\rangle$
2	3.0476(0.0000)	$0.9666\|H - 2 \rightarrow L\rangle$
3	3.1861(0.1174)	$0.9811\|H \rightarrow L\rangle$
4	3.6531(0.0018)	$0.6326\|H - 4 \rightarrow L\rangle + 0.7547\|H - 3 \rightarrow L\rangle$
5	3.8395(0.0485)	$0.7354\|H - 4 \rightarrow L\rangle - 0.6167\|H - 3 \rightarrow L\rangle$
	Alizarin$-(TiO_2)_8$	
1	1.5867(0.0021)	$-0.6466\|H \rightarrow L\rangle + 0.7423\|H \rightarrow L + 1\rangle$
2	1.6862(0.0008)	$-0.7619\|H \rightarrow L\rangle + 0.6288\|H \rightarrow L + 1\rangle$
3	2.0952(0.0002)	$-0.9327\|H - 1 \rightarrow L\rangle + 0.3191\|H - 1 \rightarrow L + 1\rangle$
4	2.1271(0.0024)	$-0.9077\|H \rightarrow L + 2\rangle + 0.2673\|H \rightarrow L + 6\rangle$
5	2.1588(0.0024)	$-0.8493\|H \rightarrow L + 3\rangle - 0.2952\|H \rightarrow L + 4\rangle$ $+0.3569\|H \rightarrow L + 6\rangle$

the typical time of the electron injection. The RT simulations indeed manifest the ET time of about a few femotoseconds. In this case, it may be reasonable to merely study the electronic dynamics and ignore the effects of nuclear motion.[28] The present work is focused on investigating the electron relaxation of photoinduced initial states in the ultrafast ET process.

2. The Numerical Approaches and Results

2.1. Electronic Structures. Several research groups did a series of work on the conformation of TiO_2 clusters theoretically.[29,30] We take the geometries of TiO_2 clusters from ref 30. $(TiO_2)_8$, $(TiO_2)_{14}$, and $(TiO_2)_{16}$ are chosen to check the dependence of the ET time on cluster size. Three chromophores, pycooh, catechol, and alizarin, are chosen to bind up with TiO_2 clusters. The relaxed compounds with the full optimization are shown in Figure 1. The optimized geometries are predicted from the Gaussian03 software package[31] the at B3LYP/Lanl2dz theory level. Lanl2dz[32] is a kind of effective core potentials which is used for Ti atoms only in this work. For atoms O, N, and H, the Pople 6-31G** basis set is used. The dyes are anchored to TiO_2 clusters in two kinds of forms. Both alizarin and catechol are adsorbed dissociatedly on the surfaces of TiO_2 clusters. The O−H bonds of dyes break up, two oxygen atoms are connected with a Ti atom, and two H atoms are separately bound to two oxygen atoms in cluster $(TiO_2)_8$. Pycooh is adsorbed on TiO_2 clusters with two types of structural models. Bound pycooh may remain intact or deprotonate, depending on the TiO_2 cluster size.

In order to investigate the interaction between the dyes and TiO_2 clusters, at first, we display the infrared spectra of dye molecules, TiO_2 clusters, and coupled systems in Figure 2. The vibrational frequencies of dye molecules and TiO_2 clusters agree well with the experimental infrared spectroscopy,[33] except those of two Ti−O single-bond stretching modes in our cluster models. The spectra of the coupled systems are obviously different from those of individual constituents that form the dye-sensitized systems, manifesting the strong coupling between them. In the short-wave region, the vibrational modes between 3100 and 3700 cm^{-1} correspond to C−H stretching motion in the dye molecules and the O−H stretching motion of H-saturated atoms on the TiO_2 clusters. The modes with wavenumbers in the range of 250−1000 cm^{-1} are related to the mixing of π-molecular orbitals of dye molecules and the d orbitals of of Ti atoms, and they dominate the interfacial ET process. The vibrational period of 33−133 fs is longer than the sub-10 fs electron injection time; 33 fs is the collective vibrational period that comes from the stretching vibration of C−C, C−O, and Ti−O bonds. It is thus acceptable to propose that the nuclei can be treated as immobile when the time of ET is as fast as several femtoseconds.

Next, we calculated the density of states (DOS) of the coupled dye−TiO_2 complexes along with their projection onto the individual constituent dyes.[34] DOS and projected DOS (PDOS) are defined as

$$\mathrm{DOS}(E) = \sum_p \delta(E - E_p) \tag{1}$$

and

$$\mathrm{PDOS(dye)}(E) = \sum_{\mu \in \mathrm{dye}} \sum_p \sum_\nu C_{\mu p} C_{\nu p} S_{\mu\nu} \delta(E - E_p) \tag{2}$$

where E_p represents the energy of the p-th molecular orbital (MO), C and S denote the MO coefficient matrix and the overlap matrix, respectively, and $\mu(\nu)$ denotes the indices of atomic orbitals. The Fermi energy is defined as the middle point of the highest occupied molecular orbital (HOMO) and the lowest unoccupied molecular orbital (LUMO). The calculation is finished with the Q-Chem software package.[35] From Figure 3, the main features of DOS can be found as follows. (1) The $(TiO_2)_8$ cluster has a HOMO−LUMO gap of 3.7 eV, which is

close to the gap of 3.4 eV in 2.4 nm TiO_2 nanoparticles[36] and the band gap of 3.2 eV in the bulk TiO_2.[5,6,37] (2) The pycooh$-(TiO_2)_x$ complex has bigger HOMO−LUMO gap (3.01 eV at $x = 8$, and 3.68 eV at $x = 16$) than the catechol$-(TiO_2)_8$ and alizarin$-(TiO_2)_8$ systems. All dyes insert states within the HOMO−LUMO gap of the TiO_2 cluster, which may create new optical excited states that are lower in energy than the TiO_2 cluster band gap absorption. However, the nearly same HOMO−LUMO gap value of the pycooh molecule as that of the TiO_2 cluster may give rise to the stronger mixing of their MOs than that in the other two sensitized systems. (3) For the catechol$-(TiO_2)_8$ and alizarin$-(TiO_2)_8$ systems, the orbitals near the HOMO and LUMO have no mixing MO characters. The HOMO − 1 and HOMO of complex nearly have the characteristics of catechol and alizarin molecules, while the lowest few virtual orbitals of the complex nearly have the same characteristics of the TiO_2 clusters. This kind of MO energy levels favors a direct optical charge transfer from catechol and alizarin to TiO_2 clusters. The visualized MOs are shown to confirm the locations of frontier MOs of dye-sensitized systems.

Finally, we calculate the low-lying electronic excitations of free dye molecules and corresponding coupled systems by using TDDFT with the Q-chem software package.[35] The results are shown in Tables 1−4. Note that the optical gaps becomes smaller after the dyes are bound to TiO_2 clusters due to the fact that the d orbitals of Ti lie below the valence orbitals of dye molecules. The biggest optical red shift of bound catechol can be observed, which can be explained by its PDOS; the LUMO of catechol lies much above the LUMO of $(TiO_2)_8$, while its HOMO and HOMO − 1 lie above the HOMO of $(TiO_2)_8$. A direct optical charge transfer from catechol or alizarin to the $(TiO_2)_8$ cluster is evidenced.

2.2. Electronic Dynamics. Now, we focus on the real-time ET process with respect to the RT-TDDFT. The time evolution of the electronic populations at the dye molecules is computed, and the lifetimes of excited adsorbate states at the finit size TiO_2 clusters are analyzed. The number of electrons on atom A at the time t is calculated as

$$P_A(t) = \sum_{\mu \in A} \sum_{\nu}^{N} \rho_{\mu\nu}(t) S_{\nu\mu} \tag{3}$$

Here, N is the number of atomic orbitals (AOs) of coupled systems, and $\rho(t)$ can be obtained by solving the TDDFT equation. In this work, the TDDFT equation is solved by propagating the reduced density matrix in the real-time domain as

$$i\hbar S \frac{d\rho(t)}{dt} S = F(t)\rho(t)S - S\rho(t)F(t) \tag{4}$$

where $F(t)$ and $\rho(t)$ represent the time-dependent Fock matrix and density matrix in the nonorthogonal AO basis, respectively. The nonorthogonal atom-centered AO basis functions can be orthogonalized by the canonical orthogonalization. In the orthogonal basis set, eq 4 becomes

$$i\hbar \frac{d\bar{\rho}(t)}{dt} = \bar{F}(t)\bar{\rho}(t) - \bar{\rho}(t)\bar{F}(t) \tag{5}$$

where $\bar{\rho} = S^{1/2}\rho S^{1/2}$ and $\bar{F} = S^{-1/2}FS^{-1/2}$. The evolution operator $U(t, t_0)$, which satisfies

$$i\hbar \frac{U(t, t_0)}{dt} = \bar{F}U(t, t_0) \tag{6}$$

is introduced into the formal solution of the density, $\bar{\rho}(t) = U(t, t_0)\bar{\rho}(t_0)U(t_0, t)$. The detailed algorithms about the equation solvers have been given in ref 26. Unlike the usual situation, the initial density matrix $\rho(t = 0)$ is obtained from a usual ground-state calculation. Here, we assume the initial state as an excited state of dye molecules, that is, the initial density matrix is built as

$$\rho(t=0) = \begin{pmatrix} \rho_e^{D-D} & \rho_0^{D-T} \\ \rho_0^{D-T} & \rho_0^{T-T} \end{pmatrix}$$

Here, ρ_e^{D-D} denotes the excited-state density matrix of the dye block, $\rho_e^{D-D} = \rho_0^{D-D} + \Delta\rho^{D-D}$. The ρ_0^{T-T} and ρ_0^{D-T} are the ground-state density matrix of the TiO_2 block and the coupled matrix of the dye−TiO_2 block, respectively. This work is concerned with the realistic computation of charge distributions, not the accurate excited-state properties. Therefore, only the one-particle density matrix $\Delta\rho$ of the dye block is added to its ground-state density matrix to generate the one-particle density matrix for an excited state. In the MO basis, it is a symmetric matrix with both occupied−occupied (OO) and virtual−virtual (VV) contributions[38]

$$\Delta\rho_{ij\sigma} = -\frac{1}{2}\sum_a [(X+Y)_{ia\sigma}(X+Y)_{ja\sigma} + (X-Y)_{ia\sigma}(X-Y)_{ja\sigma}]$$

$$\Delta\rho_{ab\sigma} = \frac{1}{2}\sum_i [(X+Y)_{ia\sigma}(X+Y)_{ib\sigma} + (X-Y)_{ia\sigma}(X-Y)_{ib\sigma}] \tag{7}$$

The vectors $|X, Y\rangle$ represent the (frequency-dependent) linear response of the density matrix in the basis of the unperturbed molecular orbitals. The total Δ one-particle density matrix for the excited state in the AO representation can be generated by transforming the entire MO basis Δ density matrix as

$$\Delta\rho_{\mu\nu} = \sum_{pq} \Delta\rho_{pq} C_{\mu p} C_{\nu q} \tag{8}$$

Here, we use the following subscript notation: μ (ν) denotes the atomic basis function, i (j) denotes the occupied MO, a (b) denotes the unoccupied MO, and p (q) denotes the generic molecular spin orbital.

With this assumption, the ET process between the dye molecules and TiO_2 clusters is thought of as a photoinduced ET process, and the electron injection is regarded as an electronic relaxation process at a very fast time scale, in which the nuclei are frozen in its equilibrium nuclear configuration. That is to say, the electrons reoptimize their locations after excitation of dyes, whereas the nuclei have no time to move. Once the initial state is specified, we can follow the time-dependent population analysis to see how the electrons are repopulated.

Figures 4 and 5 show the number of electrons localized at dye molecules versus the propagation time calculated by

$$N_{dye}(t) = \sum_{A \in dye} P_A(t) \tag{9}$$

Figure 4 is for pycooh$-(TiO_2)_{8/14/16}$, and Figure 5 is for catechol− and alizarin$-(TiO_2)_8$ systems. In this work, we are focused on the study of the electronic relaxation of low-lying excited states. The first excited states of pycooh, catechol, and alizarin are therefore chosen to construct the initial states at first. The results show that the electrons gradually depopulate the excited dye molecules, relaxing to the ground-state TiO_2 ion configuration. The time-resolved decay of electrons can be analyzed by fitting $N_{dye}(t)$ to a dual exponential function as

$$N_{dye}(t) = N_{dye}(t=0) + A_1 \exp(-t/\tau_1) + A_2 \exp(-t/\tau_2) \quad (10)$$

The exponential factors define the characteristic times of the ET events. The τ_1 with a smaller value describes an ultrafast process of the early electronic redistribution of initial states with the time scale less than 1.0 fs, while τ_2 with a larger value corresponds to the lifetime of the initial states. The τ values, which are closely related to the systems, are 0.52, 18.28; 0.51, 9.90; and 0.11, 9.14 fs for pycooh−, catechol−, and alizarin−$(TiO_2)_8$ systems, respectively. It is observed that our predicted ET times in the above three finite systems are longer than other theoretical predictions with respect to the bulk TiO_2 structures (about 5 fs in catechol−TiO_2 in ref 20 and the adiabatic ET time of 2.7 fs in pycooh−TiO_2 and 7.1 fs in alizarin−TiO_2 in ref 22) and the experimental results for pycooh−TiO_2.[39] It indicates that the cluster size has an influence on the electron injection process.

Figure 4 displays the clear dependence of the ET time on the cluster sizes. As the cluster sizes increase from $(TiO_2)_8$ to $(TiO_2)_{14}$, the τ_2 values decrease rapidly. Larger clusters $(TiO_2)_{14/16}$ show an ET time that is more consistent with the experimental measurements. However, we observe that the difference of τ values between the clusters $(TiO_2)_{14}$ and $(TiO_2)_{16}$ is small. It is

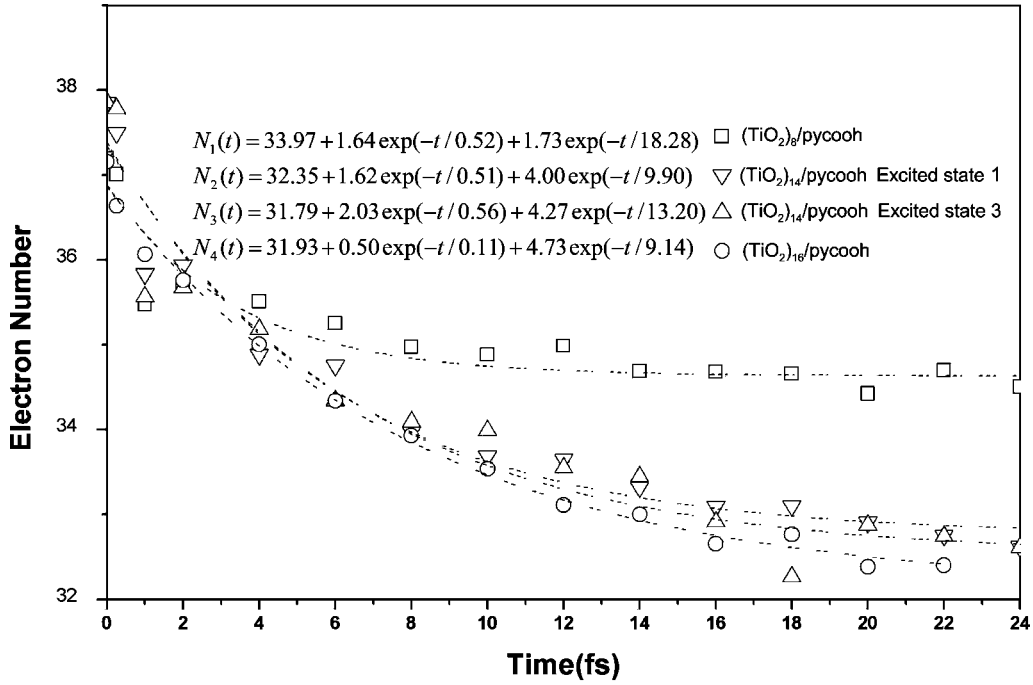

Figure 4. Electronic relaxation of the excited pycooh in the pycooh−$(TiO_2)_{8/14/16}$ systems. The number on the *y*-axis represents the number of electrons localized in pycooh. The dashed lines denote the exponential fittings.

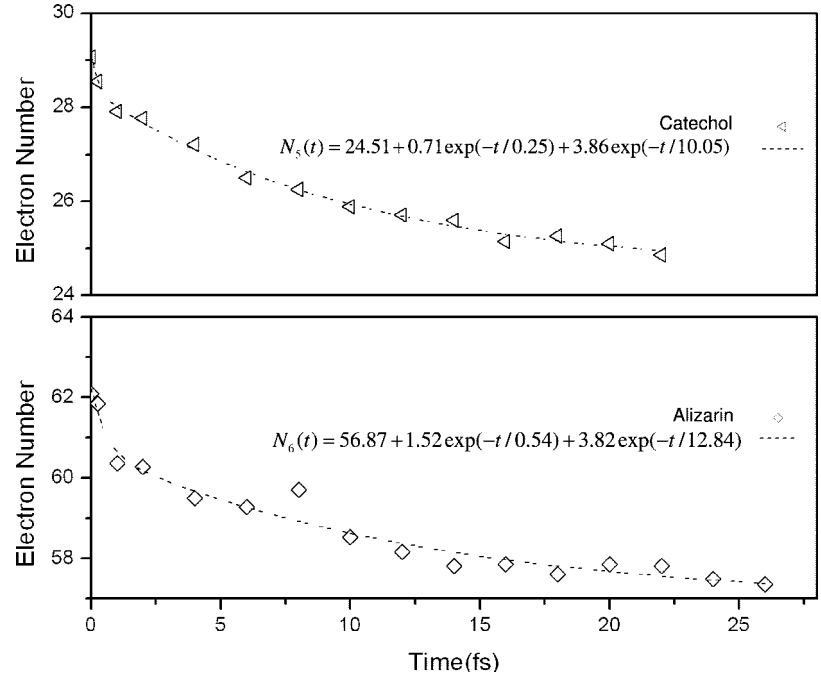

Figure 5. Electronic relaxation of the excited catechol and alizarin in $(TiO_2)_8$−catechol and $(TiO_2)_8$−alizarin systems, respectively. The dashed lines denote the exponential fittings.

thus expected that the τ value can reach a limited value when the cluster size is large enough and the 14-TiO_2 cluster model has captured the essence of electronic relaxation of the excited dyes at an affordable computational cost, although a larger cluster or periodic system is, of course, always more accurate.

In the above description of the dynamic process, we choose the first excited state of dye molecules to construct the initial state of the ET process. The reason is as follow. The first excited state of the complex is an ET state, which comes from the transitions from HOMO and HOMO − 1 to LUMO. From the PDOS in Figure 3, it is found that the HOMO and HOMO − 1 are located by dye molecules, while the LUMO is located by TiO_2 clusters. The transitions of HOMO → LUMO and HOMO − 1 → LUMO only involve the contribution of occupied molecular orbitals of dye molecules to unoccupied molecular orbitals of TiO_2 clusters. Therefore, our choice of initial density matrix is an acceptable approximation to represent the photoinduced electron injection from the excited adsorbates to TiO_2 clusters.

To show the influence of initial states on the ET event, we use the different initial states to start integrating the TDDFT equation. As an example, pycooh's first excited state (which nearly fully comes from the electron transitions from HOMO → LUMO) and the third excited state (which comes mainly from the HOMO − 1 → LUMO and HOMO − 3 → LUMO transitions) will be chosen to construct the different initial states. These two excited states are both optically active. It is observed that the electronic relaxing times starting from the different initial state are different. The initial state built from the first excited state of pycooh favors a faster ET than the one built from the thirrd excited state of pycooh. From the orbital contributions of low-lying excited states for the pycooh−$(TiO_2)_{14}$ system listed in Table 2, we note that they come mainly from the orbital transitions from the occupied HOMO or HOMO − 1 of pycooh to the virtual orbitals of $(TiO_2)_{14}$. These states are the direct optical charge-transfer states. Thus, the time scale of the direct optical ET is fastest in the ET process. The third excited state of pycooh involves the orbital contribution from HOMO − 3 → LUMO, which slows down the ET event between the excited pycooh and $(TiO_2)_{14}$. However, both initial states behave nearly in the same time-dependent character since the contribution to the third excited state of pycooh from the HOMO − 3 → LUMO transition is much smaller than that from HOMO − 1 → LUMO.

3. Concluding Remarks

We have combined quantum chemistry calculations and ab initio electronic dynamics numerical simulations to investigate the ultrafast electron transfer across the dye-sensitized interface. The calculated DOS/PDOS, IR spectra and low-lying excited states demonstrate that the coupling between dyes and the TiO_2 cluster is very strong, which favors an ultrafast ET process between them. Our ab initio electron dynamics simulation gives evidence that the electron injection from the excited dyes to TiO_2 is an ultrafast process. We have reproduced the experimentally observed ET features and demonstrate that the dye−TiO_2 cluster model can correctly describe the photoinduced ET in the dye−TiO_2 systems. The ET process is significantly influenced by the cluster size when the cluster is small. However, the size effects on ET time reduce dramatically as the cluster size increases. A moderate middle size cluster $(TiO_2)_{14}$ has captured the essence of electronic relaxation of the excited dyes to the TiO_2 cluster at an affordable computational cost. It is expected to reproduce the experimental or other theoretical results for the bulk TiO_2 when the cluster size is large enough. Our results also indicate that it is safe to ignore the nuclear movement for the present systems because its relaxation time is about subpicoseconds.

Acknowledgment. Financial support from the National Science Foundation of China (Nos. 20673104 and 50121202) and a 973 project funded by National Basic Research Program of China (Nos: 2004CB719901 and 2006CB922004) are acknowledged.

References and Notes

(1) Miller, R. J. D.; Gclendon, G.; Nozik, A. J.; Schimickler, W.; Willig, F. *Surface Electron Transfer Processes*; VCH: New York 1995.
(2) Burfeindt, B.; Hannappel, T.; Storck, W.; Willig, F. *J. Chem. Phys.* **1996**, *100*, 16463.
(3) Onda, K.; Li, B.; Zhao, J.; Jordan, K. D.; Yang, J. L.; Petek, H. *Science* **2005**, *308*, 1154.
(4) Li, B.; Zhao, J.; Onda, K.; Jordan, K. D.; Yang, J. L.; Petek, H. *Science* **2006**, *311*, 1436.
(5) Zhao, J.; Li, B.; Onda, K.; Feng, M.; Petek, H. *Chem. Rev.* **2006**, *106*, 4402.
(6) Gundlach, L.; Ernstorfer, R.; Willig, F. *Prog. Surf. Sci.* **2007**, *82*, 355.
(7) Zhao, W.; Ma, W. H.; Chen, C. C.; Zhao, J. C.; Shuai, Z. G. *J. Am. Chem. Soc.* **2004**, *126*, 4782.
(8) Kim, H. G.; Hwang, D. W.; Lee, J. S. *J. Am. Chem. Soc.* **2004**, *126*, 8912.
(9) Huang, W. Y.; Yu, Y. *Prog. Chem.* **2005**, *17*, 242.
(10) O'Regan, B.; Grätzel, M. *Nature* **1991**, *353*, 737.
(11) Grätzel, M. *Nature* **2001**, *414*, 338.
(12) Hannappel, T.; Burfeindt, T.; Storck, W.; Willig, F. *J. Phys. Chem. B* **1997**, *101*, 6799.
(13) Willig, F.; Zimmermann, C.; Ramakrishna, S.; Storck, W. *Electrochim. Acta* **2000**, *45*, 4565.
(14) Tachibana, Y.; Moser, J. E.; Grätzel, M.; Klug, D. R.; Durrant, J. R. *J. Phys. Chem. B* **1996**, *100*, 20056.
(15) Asbury, J. B.; Hao, E. C.; Wang, Y. Q.; Ghosh, H. N.; Lian, T. Q. *J. Phys. Chem. B* **2001**, *105*, 4545.
(16) Anderson, N. A.; Lian, R. Q. *Annu. Rev. Phys. Chem.* **2005**, *56*, 491.
(17) Ramakrishna, S.; Willig, F. *J. Phys. Chem. B* **2000**, *104*, 68.
(18) Wang, L. X.; May, V. *J. Chem. Phys.* **2004**, *121*, 8039.
(19) Thoss, M.; Kondov, I.; Wang, H. *Chem. Phys.* **2004**, *304*, 169.
(20) Rego, L. G. C.; Batista, V. S. *J. Am. Chem. Soc.* **2003**, *125*, 7989.
(21) Duncan, W. R.; Stier, W. M.; Prezhdo, O. V. *J. Am. Chem. Soc.* **2005**, *127*, 7941.
(22) Duncan, W. R.; Prezhdo, O. V. *Annu. Rev. Phys. Chem.* **2007**, *58*, 143.
(23) Memming, R. *Semiconductor Electrochemistry*; Wiley-VCH: Weinheim, Germany, 2007.
(24) Muscat, J.; Swamy, V.; Harrison, V. M. *Phys. Rev. B* **2002**, *65*, 224112.
(25) Zhang, H.; Banfield, J. F. *J. Mater. Chem.* **1998**, *8*, 2073.
(26) Sun, J.; Song, J.; Zhao, Y.; Liang, W. Z. *J. Chem. Phys.* **2007**, *127*, 234107.
(27) Wang, F.; Yam, C. Y.; Chen, G. H. *J. Chem. Phys.* **2007**, *126*, 244102.
(28) Ramacle, F.; Levine, R. D. *Proc. Natl. Acad. Sci. U.S.A.* **2006**, *103*, 6793.
(29) Qu, Z. W.; Kroes, G. J. *J. Phys. Chem. B* **2006**, *110*, 8998.
(30) Lundqvist, M. J.; Nilsing, M.; Persson, P.; Lunell, S. *Int. J. Quantum Chem.* **2006**, *106*, 3214.
(31) Frisch, M. J. Trucks, G. W.; Schlegel, H. B.; Scuseria, G. E.; Robb, M. A.; Cheeseman, J. R.; Montgomery, J. A., Jr.; Vreven, T.; Kudin, K. N.; Burant, J. C.; Millam, J. M.; Iyengar, S. S.; Tomasi, J.; Barone, V.; Mennucci, B.; Cossi, M.; Scalmani, G.; Rega, N.; Petersson, G. A.; Nakatsuji, H.; Hada, M.; Ehara, M.; Toyota, K.; Fukuda, R.; Hasegawa, J.; Ishida, M.; Nakajima, T.; Honda, Y.; Kitao, O.; Nakai, H.; Klene, M.; Li, X.; Knox, J. E.; Hratchian, H. P.; Cross, J. B.; Bakken, V.; Adamo, C.; Jaramillo, J.; Gomperts, R.; Stratmann, R. E.; Yazyev, O.; Austin, A. J.; Cammi, R.; Pomelli, C.; Ochterski, J. W.; Ayala, P. Y.; Morokuma, K.; Voth, G. A.; Salvador, P.; Dannenberg, J. J.; Zakrzewski, V. G.; Dapprich, S.; Daniels, A. D.; Strain, M. C.; Farkas, O.; Malick, D. K.; Rabuck, A. D.; Raghavachari, K.; Foresman, J. B.; Ortiz, J. V.; Cui, Q.; Baboul, A. G.; Clifford, S.; Cioslowski, J.; Stefanov, B. B.; Liu, G.; Liashenko, A.; Piskorz, P.; Komaromi, I.; Martin, R. L.; Fox, D. J.; Keith, T.; Al-Laham, M. A.; Peng, C. Y.; Nanayakkara, A.; Challacombe, M.; Gill, P. M. W.; Johnson,

B.; Chen, W.; Wong, M. W.; Gonzalez, C.; Pople, J. A. *Gaussian 03*, revision D.01; Gaussian, Inc.: Wallingford, CT, 2004.

(32) Hay, P. J.; Wadt, W. R. *J. Chem. Phys.* **1985**, *82*, 299.

(33) Gonzalez, R. J.; Zallen, R. *Phys. Rev. B* **1997**, *55*, 4014.

(34) Hoffmann, R. *Solids and Surfaces: A Chemist's View of Bonding in Extended Structures*; VCH: New York 1988.

(35) Shao, Y.; Molnar, L. F.; Jung, Y.; Kussmann, J.; Ochsenfeld, C.; Brown, S. T.; Gilbert, A. T. B.; Slipchenko, L. V.; Levchenko, S. V.; O'Neill, D. P.; DiStasio, R. A.; Lochan, R. C.; Wang, T.; Beran, G. J. O.; Besley, N. A.; Herbert, J. M.; Lin, C. Y.; Van Voorhis, T.; Chien, S. H.; Sodt, A.; Steele, R. P.; Rassolov, V. A.; Maslen, P. E.; Korambath, P. P.; Adamson, R. D.; Austin, B.; Baker, J.; Byrd, E. F. C.; Dachsel, H.; Doerksen, R. J.; Dreuw, A.; Dunietz, B. D.; Dutoi, A. D.; Furlani, T. R.; Gwaltney, S. R.; Heyden, A.; Hirata, S.; Hsu, C. P.; Kedziora, G.; Khalliulin, R. Z.; Klunzinger, P.; Lee, A. M.; Lee, M. S.; Liang, W.; Lotan, I.; Nair, N.; Peters, B.; Proynov, E. I.; Pieniazek, P. A.; Rhee, Y. M.; Ritchie, J.; Rosta, E.; Sherrill, C. D.; Simmonett, A. C.; Subotnik, J. E.; Woodcock, H. L.; Zhang, W.; Bell, A. T.; Chakraborty, A. K.; Chipman, D. M.; Keil, F. J.; Warshel, A.; Hehre, W. J.; Schaefer, H. F.; Kong, J.; Krylov, A. I.; Gill, P. M. W.; Head-Gordon, M. *Phys. Chem. Chem. Phys.* **2006**, *8*, 3172.

(36) Kormann, C.; Bahnemann, K. W.; Hoffmann, M. R. *J. Phys. Chem.* **1988**, *92*, 5196.

(37) Tang, H.; Levy, F.; Berger, H.; Schmid, P. E. *Phys. Rev. B* **1995**, *52*, 7771.

(38) Scalmani, G.; Frisch, M. J.; Mennucci, B.; Tomasi, J.; Cammi, R.; Barone, V. *J. Chem. Phys.* **2006**, *124*, 094107.

(39) Scnadt, J.; Brühwiler; P, A.; Patthey, L.; O'Shea, J. N.; Södergren, S.; Odelius, M.; Ahuja, R.; Karis, O.; Bässler, M.; Persson, P.; Slegbahn, H.; Lunell, S.; Martensson, N. *Nature* **2002**, *418*, 620.

JP802007H